Volume 14
Number 44
28 November 2023
Pages 4943-5022

Polymer Chemistry

rsc.li/polymers

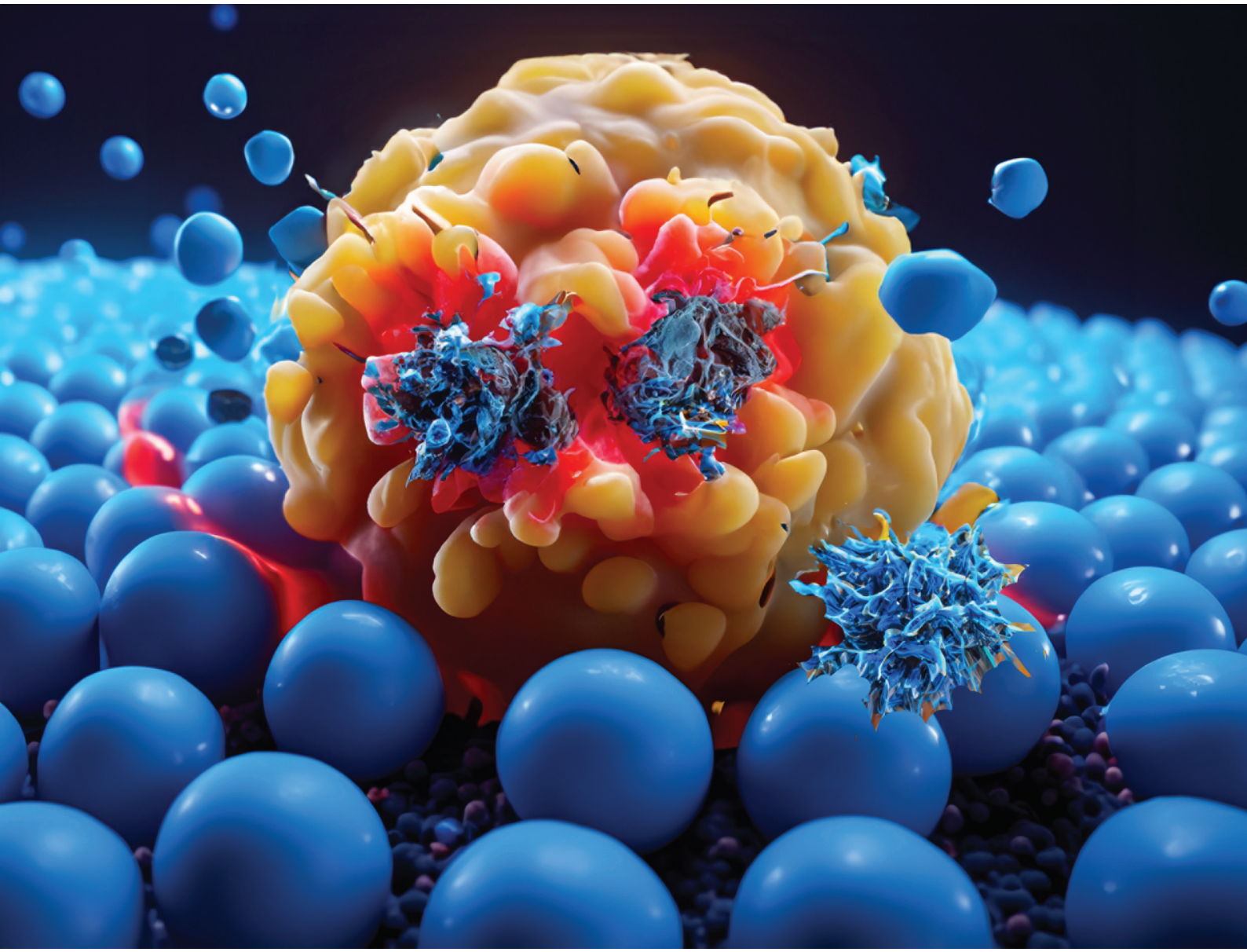

ISSN 1759-9962

ROYAL SOCIETY OF CHEMISTRY

PAPER

James F. Reuther *et al.*

Multi-responsive nanogels with tunable orthogonal reversible covalent (TORC) core-crosslinks for AND-gate controlled release

Polymer Chemistry

ROYAL SOCIETY OF CHEMISTRY

PAPER

View Article Online
View Journal | View Issue

Cite this: *Polym. Chem.*, 2023, **14**, 4957

Multi-responsive nanogels with tunable orthogonal reversible covalent (TORC) core-crosslinks for AND-gate controlled release†

Shayesteh Tafazoli, Ali Shahrokhinia, Sahaj Rijal, Jaelese Garay, Randall A. Scanga and James F. Reuther *

Received 8th August 2023,
Accepted 29th September 2023

DOI: 10.1039/d3py00922j

rsc.li/polymers

Smart, multi-stimuli-responsive nanogels that possess dynamic covalent bonds (DCBs) exhibit reversibility under equilibrium conditions allowing for controlled disassembly and release of cargo. These nanomaterials have innumerable applications in areas including drug delivery, sensors, soft actuators, smart surfaces, and environmental remediation. In this work, we implement one-pot, photo-controlled atom transfer radical polymerization-induced self-assembly (PhotoATR-PISA), mediated by UV light (λ = 365 nm) and parts per million (ppm) levels (*ca.* <20 ppm) of a copper(II) bromide catalyst, to fabricate dual crosslinked, polymeric nanogels with tunable orthogonal reversible covalent (TORC-NGs) core-crosslinks (CCLs). These TORC-NGs were crosslinked efficiently *via* coumarin photodimerization which occured simultaneously during polymerization using coumarin-functionalized methacrylate crosslinkers (CouMA). At the same time, crosslinking of nanocarriers with *N*,*N*-cystamine bismethacrylamide (CBMA) introduced orthogonal, redox-responsive, disulfide CCLs. Furthermore, incoproration of poly(glycidyl methacrylate) (PGMA) core-forming segments provided a simple handle for switchable solubility through acid-catalyzed ring-opening hydrolysis of pendant epoxide groups. In this way, the kinetics of release were tailored by the pH of the surrounding media. Thus, these TORC-NG systems showed coupled pH-, redox- and photo-responsive controlled release and disassembly behavior with full release of cargo only observed in the right sequence of stimuli and only when all three are utilized. The multi-stimuli-responsive nature of these TORC-NGs was successfully utilized herein for the controlled encapsulation and on-demand AND-gate release of hydrophobic Nile Red fluorescent reporters used as drug simulants. Various TORC-NG morphologies were synthesized in this report including nanosphere, worm-like and tubesome NGs showing variable release characteristics.

Introduction

Next-generation smart materials fabricated with stimuli-responsive polymers have been intensely investigated for applications such as drug delivery,[1] catalysis,[2] separations,[3] sensors,[4] actuators,[5] Pickering emulsions,[6] to name a few. Amphiphilic block copolymers with stimuli-responsive components are of particular interest among various polymeric systems for two key reasons: (1) they can self-assemble into diverse supramolecular structures with interiors (cores) that can non-covalently encapsulate cargo molecules, and (2) the release of cargo molecules can be triggered by external stimuli.[7] Therefore, physical, chemical, biological, or environmental stimuli can be used to specifically modulate their physical, chemical, and biological properties and, therefore, their functions.[8,9] However, specifically switching on and off the release of the encapsulated cargo molecules in response to changing environmental conditions remains a challenging endeavor. Tunable Orthogonal Reversible Covalent (TORC) bonds are reversible covalent bonds with orthogonal reactivity allowing for dynamic covalent exchange in one-pot without cross-reactivity between non-complementary bonding pairs.[10] In some cases, TORC bonds can reversibly break and reform in response to external stimuli (*e.g.*, heat, light, pH, redox). TORC bonds must be tunable in nature, in that they can be replaced with other, similar functionalities to change the kinetics and thermodynamics of reversibility.[11,12] Furthermore, due to their orthogonal and reversible natures, non-complementary TORC bonds must show no reactivity. Finally, the robust properties of covalent bonds advance the materials applicability of these interactions beyond traditional supramolecular chemistry.

Department of Chemistry, University of Massachusetts Lowell, Lowell, MA 01854, USA. E-mail: james_reuther@uml.edu

†Electronic supplementary information (ESI) available: Additional characterization, methods and analysis. See DOI: https://doi.org/10.1039/d3py00922j

TORC bonding has reported uses in a wide range of disciplines,[13–15] particularly biomedical applications.[16] When multiple TORC bonding pairs are combined, extraordinarily high levels of chemical sophistication and assembly can be accomplished resulting in advances that range from chemical sensing to molecular machines to predicted information storage.[11,17,18] Thus, polymer nanomaterials that utilize multiple TORC bonds in unison to accomplish light, redox, and pH-responsivity can yield unique, synergistic, multi stimuli-responsive materials in many of the aforementioned applications.

The non-destructivity, facile applicability, tunable intensity/wavelength, and temporal/spatial control are all advantages of incorporating light responsive moieties.[19–23] Coumarin functional groups can demonstrate reversible dimerization in response to UV-A light (λ = 365 nm) *via* [2 + 2] cycloaddition reactions and dissociation in response to UV-C light (λ = 254 nm). This reversible coupling/decoupling responsiveness has been utilized in various applications such as light-induced crosslinking of polymer matrices,[24,25] core and shell crosslinking in self-assembled polymer nanoparticles,[26–29] light-responsive rheological modifiers,[30] self-healing materials,[31,32] and photo-degradable hydrogels.[29,33,34]

Redox-responsive, cleavable disulfide crosslinkers are prevalently used to crosslink polymeric particles in biological applications[35] such as drug delivery,[36–39] anti-bacterial gels,[40] bioadhesives,[41] and energy storage,[42] to name a few. Crosslinking cores and/or shells of nanoparticles is utilized heavily in drug delivery disciplines to improve the structural stability of nanocarriers and reduce long-term toxicity *via* unwanted nanocarrier degradation and subsequent metabolism of the degradation products.[43,44] In order to accomplish precise on/off release of the cargo in response to external stimuli, TORC-based chemical crosslinkers can be incorporated to enable the system to respond to specific cues based on the simple principle of Boolean logic "YES", "AND", or "OR". An example of AND-gate crosslinked systems require two different stimuli-responsive units connected in parallel in which the presence of a single input alone does not fully sever the crosslinkers as a whole requiring two inputs for full release.[1,45–52]

DeForest and coworkers reported an impressive achievement in which they designed 17 distinct stimuli-responsive crosslinkers ("logic gates") and synthesized several PEG-based hydrogels that responded to specific cues based on enzyme AND reductant gates. The hydrogel remained intact in the absence of treatment, or in the presence of GSH or the enzyme matrix metalloproteinase-8 (MMP-8) alone, resulting in normal cell proliferation. Combined presence of GSH and MMP-8 resulted in the release of DOX from the hydrogels and the elimination of HeLa cells.[53] Almutairi *et al.* created a pH and oxidation–responsive nanoparticle made of polythioether ketal that decomposes in response to reactive oxygen species (ROS) and acidic pH. Following ROS exposure, the polymeric backbone changed from hydrophobic to hydrophilic, allowing for rapid acid-catalyzed ketal group degradation in mildly acidic environments.[54]

Various polymerization methods have been employed in the fabrication of multi-stimuli responsive polymer nanoparticles. Polymerization-induced self-assembly (PISA) has received much interest due to its unique ability to form polymer nanoparticles *in situ* at high solids concentrations simultaneously during polymerization.[55,56] When compared to traditional self-assembly, the primary benefits of PISA are enhanced scalability, morphological tunability, and simplified, streamlined syntheses.[57–59] *In situ* crosslinking of nanoparticles employing monomers with multiple vinyl groups may be preferable to post-polymerization crosslinking methods because stabilized nanoparticles can be prepared directly. This approach, however, is difficult because significantly reducing chain mobility during the crosslinking procedure limits access to higher-order morphology such as vesicles. Furthermore, crosslinkers with high reactivity can lead to uncontrolled network formation rather than controlled nanoparticle CCL.[60]

The emergence of newly developed photo-controlled atom transfer radical polymerization (PhotoATRP) methodologies have enabled one-pot polymeric synthesis of multiblock copolymers with up to 23 different blocks *via* controlled chain extensions at high monomer conversions with low concentrations of copper catalyst.[61,62] When combining PhotoATRP with PISA (*i.e.*, PhotoATR-PISA), our group has previously demonstrated the facile incorporation of functionalized end-groups, *in situ* synthesis of different nanoparticle morphologies at room temperature using parts per million (ppm) levels (*ca.* <20 ppm) of copper catalyst, temporal control over sequential chain extensions, access to record-high solids concentrations for PISA dispersions (*ca.* SC% = 79 w%) and rapid crosslinking of functional end-groups to form adsorbent nanoparticle network materials.[63–65]

Herein, utilizing PhotoATR-PISA mediated by UV light (λ = 365 nm), we demonstrate the *in situ* synthesis of varied nanostructured morphologies, ranging from nanospheres to worm-like micelles to tubesomes, with two TORC-based CCLs incorporated simultaneously. A series of well-defined, TORC-CCL polymeric nanogels (TORC-NGs) were prepared using solvophilic poly(oligo(ethylene glycol) methyl ether methacrylate) (POEGMA) macroinitiators chain extended with poly(glycidyl methacrylate) (PGMA) or poly(benzyl methacrylate) (PBMA) as the core-forming segments and *N*,*N*-cystamine bismethacrylamide (CBMA) and coumarin-methacrylate (CouMA) as TORC-crosslinkers. The complementary wavelength of PhotoATR-PISA and the photodimerization of coumarin allowed for facile incorporation of UV-responsive TORC-CCLs to couple with the redox-responsive disulfide CCLs from CBMA. In addition to the TORC-CCLs, the incorporation of PGMA segments provides switchable solubility in the cores of nanostructures enabled by the acid-catalyzed ring-opening hydrolysis of epoxide pendant groups; a feature that is required for full TORC-NG disassembly (Fig. 1).

Each component of the TORC-NGs has been previously studied for biocompatibility with all polymers meeting the cri-

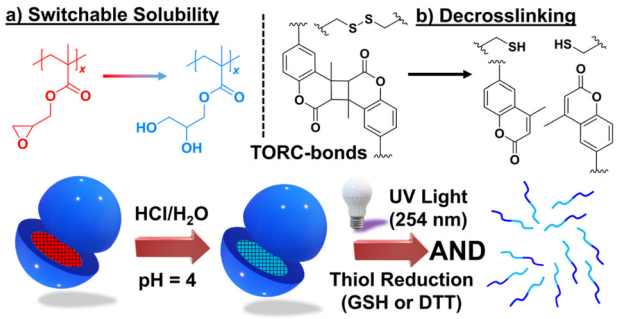

Fig. 1 Multi-responsive TORC-NG materials, synthesized in one-pot *via* PhotoATR-PISA, which can fully disassemble only when first exposed to acidic aqueous environments (pH = 4; a) followed by UV-C irradiation (λ = 254 nm) and thiol reducing agents (b).

teria apart from PGMA.[66–68] Depending on the desired administration of the nanogels, the core of nanostructures can be hydrolyzed prior to treatment providing biocompatible PGlyMA cores. These TORC-NGs were loaded with Nile Red to enable quantitative evaluation of release behavior in response to various stimuli including UV-C light (λ = 254 nm), disulfide reducing agents (*e.g.*, dithiothreitol or DTT, glutathione or GSH) and acidic pH. Fluorescence spectroscopy verified Nile red encapsulation and release. It was shown that each mentioned stimuli could trigger Nile red release to some extent with AND-gate release behaviors during simultaneous stimuli-application required for full cargo release. Furthermore, we demonstrate that the rate of release could be tuned by varying the morphology of TORC-NG. The kinetics of release could also be tailored by the pH of the surrounding medium. Furthermore, introduction of stimuli in specific orders provided enhanced release efficiencies with only full cargo release observed when the TORC-NGs are exposed to acidic environments prior to AND-gate application of UV-light and thiol-reducing agents. Finally, replacing PGMA with PBMA core-forming segments was required to form vesicle TORC-NGs with the surprising evolution of these structures to CCL tubesome TORC-NGs.

Experimental section

Materials

Cupric bromide (Cu(II)Br_2, 99%, Sigma-Aldrich), propargyl alcohol (Sigma-Aldrich), triethylamine (Fisher Sci), 2-bromoisobutyryl bromide (Sigma-Aldrich), cystamine dihydrochloride (Sigma-Aldrich), methacryloyl chloride (Fisher Scientific), coumarin methacrylate (Sigma-Aldrich), and tris(pyridin-2-ylmethyl) amine (TPMA, TCI America), tris[2-(dimethylamino) ethyl]amine (Me_6TREN, Sigma-Aldrich) were used as received. All solvents have been purchased from Fish er Scientific, which were used as received. HPLC-grade THF was purchased (Fisher Scientific) and used as received for GPC analysis. Prior to use, oligo(ethylene oxide) methyl ether methacrylate (OEGMA, M_n = 300 Da, Sigma-Aldrich), benzyl methacrylate (BMA; Alfa Aesar), and glycidyl methacrylate (GMA; Alfa Aesar) were passed through a column of basic alumina to remove inhibitor. Synthesis of CBMA,[56] CouMA (SI)[69] and alkyne-ATRP initiator[70] was adapted from previously reported literature.

A XICHEN 36 W UV nail gel curing lamp (available from a variety of suppliers such as WalMart or eBay) (max 360 nm) with four 9 W bulbs was used for all polymerizations.

Spherical TORC-NG synthesized using one-pot PhotoATR-PISA

Purified OEGMA monomer (1.0 mL, 3.5 mmol, 40 eq.), alkyne-based ATRP initiator (17.9 mg, 0.0875 mmol, 1.0 eq.), $CuBr_2$ (0.195 mg, 0.875 μmol, 0.01 eq.), TPMA (1.01 mg, 3.50 μmol, 0.04 eq.), DMF (internal standard; 58.3 μL, 0.753 mmol), and 10.7 mL of MeOH were added to a 6-dram vial. The reaction solution was than sparged with nitrogen for 15 min and the polymerization was initiated by placing the degassed reaction mixture under the UV lamp. To maintain end-group fidelity, the POEGMA polymerization was continued until ~60–70% OEGMA conversion. Then, after degassing for 15 minutes with a nitrogen-purged syringe, the monomer for the second block, GMA (7.53 mmol, 1.0 mL, 86 eq.), with both crosslinkers (CouMA and CBMA) at molar ratio 3.0 mol% with respect to GMA (67.1 mg, 0.233 mmol and 67.0 mg, 0.233 mmol, respectively) were injected to the system (solids concentration = SC% = 25 w%). Periodically, samples were collected for kinetic and conversion analysis *via* ^{1}H NMR and GPC. Calculations of monomer conversion were made relative to internal standards (DMF). Moreover, one control system without any crosslinkers was synthesized using the same procedure without added crosslinker targeting DP(PGMA) = 86, SC% = 25%.

Worm-like TORC-NG synthesized using one-pot PhotoATR-PISA

To synthesize higher order worm-like TORC-NGs, our previously demonstrated sequential chain extension strategy was applied.[70] In brief, the procedure outlined above was repeated up until the adding of GMA. Prior to addition of crosslinkers, one initial batch of degassed GMA (7.53 mmol, 1.0 mL, 86 eq.), was introduced into the system under UV irradiation; afterward, at ~60–70% conversion of first batch, second part of degassed GMA (3.76 mmol, 0.5 mL, 43 eq.) for further chain extension the gradient copolymers with both crosslinkers (CouMA and CBMA) at molar ratio 2.0 mol% with respect to GMA (66.4 mg, 0.230 mmol and 66.3 mg, 0.230 mmol, respectively) were added into the system (final solid content = 25 w%). The reaction continued under UV irradiation until full conversion and the reaction was quenched upon exposure to air. The higher DP(PGMA) = 129 and SC% = 25% led to the formation of beaded worm aggregates as evidenced by TEM.

Tubesome-based TORC-NG from two-pot PhotoATR-PISA

For the synthesis of higher-order vesicle-based TORC-NG, two main differences were employed: (1) formation of block copolymers *via* two-pot PhotoATR-PISA and (2) use of BMA core-

forming blocks. Firstly, purified OEGMA monomer (5.0 mL, 17.5 mmol, 40 eq.), alkyne-based ATRP initiator (97.7 mg, 0.4375 mmol, 1.0 eq.), $CuBr_2$ (2.30 mg; 10.5 μmol; 0.02 eq.), Me_6TREN (14.5 mg; 62.9 μmol), DMF (internal standard; 325 μL, 4.2 μmol), and 5.0 mL of solvent, 2,2,2-trifluoroethanol (TFE), were added to a septum sealed vial and degassed with nitrogen for 15 min. The polymerization started upon placing the degassed reaction mixture under the UV irradiation and was quenched at ~60–70% POEGMA conversion to preserve end-group fidelity. After removing TFE by rotary evaporation, the macroinitiator was diluted a small amount of DCM (~2 mL) and passed through a column of neutral alumina to remove residual copper catalyst. Then, excess DCM was removed by rotary evaporation and the viscous macroinitiator was precipitated from cold diethyl ether : hexanes mixture (50 : 50 by volume).

Subsequently, the desired amount of macroinitiator (M_n = 5.41 kDa, 408 mg, 75.4 μmol), BMA (3.20 mL, 18.9 μmol, 250 eq.), Nile Red (0.01 mol% relative to BMA), and CBMA (54.9 mg, 0.191 mmol, 2.5 eq.) were dissolved in DMF (0.905 mL). $CuBr_2$ (0.168 mg, 0.754 μmol), TPMA (0.876 mg, 3.02 μmol), and the required amount of methanol according SC% = 31 w% were added to the septum sealed vial and degassed by purging with nitrogen for 15 min. The polymerization was then started upon placing the degassed reaction mixture under UV irradiation monitoring monomer conversion *via* ^{1}H NMR until ~50% PBMA conversion. At this time, CouMA (54.9 mg, 0.191 mmol, 2.5 eq.) in DMF (0.710 mL) was injected to the system after degassing for 15 min *via* a nitrogen purged syringe. The reaction proceeded under UV irradiation until full monomer conversion for PhotoATR-PISA and was terminated upon exposure to air. Samples were taken periodically and analysed using ^{1}H NMR and GPC for kinetic analysis. TEM and DLS were used to investigate morphology evolution and particle size, respectively.

In situ encapsulation of Nile red and release study

Nile red was dissolved in GMA or BMA and integrated into NP during polymerization for the Nile Red release studies (0.01 mol% relative to GMA). At the end of polymerization, dialysis against water was carried out to remove the unencapsulated Nile red. The following cargo release protocol was applied to all materials investigated herein.

To study the release behavior, 0.5 mL of the reaction aliquot in water, containing Nile red loaded CCL NPs, was taken, split into four separate vials, and diluted to 5.0 mg mL^{-1}. For two experiments, the solution pH was adjusted to pH = 4 upon titration with hydrochloric acid solution (1 M), while two were maintained at pH = 7. To one CCL NP solution at pH = 4 and one at pH = 7, DTT or GSH were added as redox triggers to dissociate disulfide CBMA crosslinks. All four solutions were incubated and stirred at ambient temperature for 72 h, while the emission intensity changes at λ = 600 nm were monitored over different time intervals. For UV-responsiveness the same solutions just exposed to UV light (λ = 254 nm) to decrosslink the CouMA CCLs.

Results and discussion

Synthesis multi-stimuli responsive TORC-NG *via* PhotoATR-PISA

To incorporate stimuli-responsiveness from orthogonal stimuli (*i.e.*, UV, redox and pH), three key features were incorporated into the TORC-NG microstructure. The presence of hydrophobic PGMA cores with reactive epoxide pendant groups provide pH responsive switchable solubility *via* ring-opening hydrolysis. Furthermore, simultaneous CCL procedures using CouMA and CBMA crosslinkers provide UV- and redox-responsive moieties, respectively (Scheme 1).

Firstly, the alkyne-functionalized ATRP initiator was synthesized based on a previous report[70] *via* the esterification of 2-bromoisobutyryl bromide with propargyl alcohol. These alkyne-functionalities decorate TORC-NGs with reactive groups which will be utilized in future applications such as attaching receptors for targeted drug delivery and performing inter-nanoparticle crosslinking reactions to generate porous hydrogels for tissue engineering. Furthermore, this external functionality can be utilized to incorporate other polymers to access different morphologies.

Hydrophilic POEGMA blocks were synthesized in the first, one-pot step to act as the soluble macroinitiator for subsequent PhotoATR-PISA in methanol. PhotoATR-PISA implements $CuBr_2$/TPMA catalyst systems and commercial gel nail Polish UV curing lamp (λ_{max} = 365 nm). For all described TORC-NG systems, we targeted DP = 40 for POEGMA using optimized $CuBr_2$/TPMA catalyst concentrations from our previous report.[56] The polymerization of hydrophobic GMA monomers was then initiated in the same reaction vessel after ~70% OEGMA conversion to preserve chain-end integrity. To synthesize different morphologies, the DP of GMA varied between 86 and 129, keeping solids concentration constant at SC% = 25%. Furthermore, as a drug model, Nile red, a hydrophobic fluorescent indicator, was dissolved in GMA (0.01 mol% relative to GMA) and added to the reaction vessel to efficiently encapsulate the cargo during polymerization and assembly. Following synthesis and assembly, all TORC-NGs and controls were purified *via* dialysis to remove any unbound Nile Red and to transfer the nanoparticles to aqueous dispersions.

In situ TORC-CCLs were then incorporated in one pot *via* copolymerization with divinyl comonomers following PhotoATR-PISA providing a straightforward and convenient method to afford stabilized, multi-responsive TORC-NGs.[71–73] For spherical TORC-NG morphologies, PhotoATR-PISA was conducted at target DP(PGMA) = 86 from POEGMA macroinitiators (DP = 24 based on ^{1}H NMR at time of GMA addition) with GMA, CouMA and CBMA (*ca.* target DP(CBMA + CouMA) = 5.0) crosslinkers added at ~70% POEGMA conversion. For worm-like TORC-NGs, we targeted DP(PGMA) = 129 with the same target DP(CBMA + CouMA) = 5.0. For this, the GMA monomer was added in two batches with both crosslinkers introduced with the second addition of GMA after ~70% conversion to allow for morphological evolution to take place. Moreover, one control system without any crosslinkers was

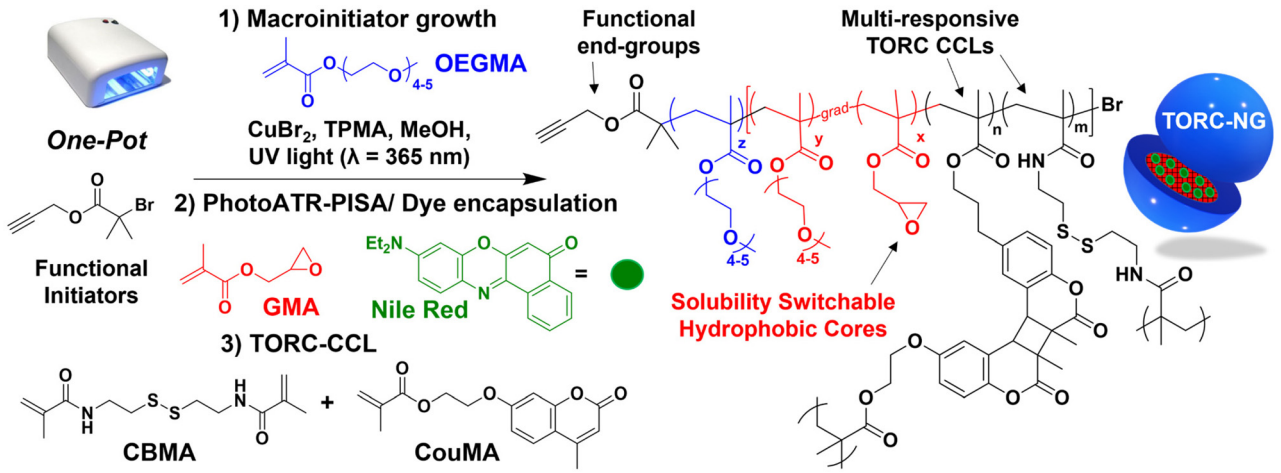

Scheme 1 Synthesis of Nile Red encapsulated, light/redox/acid-responsive gradient copolymer TORC-NG *via* one-pot, PhotoATR-PISA using redox-responsive CBMA crosslinker with disulfide bonds, UV-responsive CouMA crosslinkers and pH sensitive, PGMA hydrophobic cores.

synthesized using the same PhotoATR-PISA condition with target DP(PGMA) = 86.

The ^{1}H NMR and gel permeation chromatography (GPC) analysis of the POEGMA-*b*-[POEGMA-grad-PGMA] (Fig. S1–S9†) confirmed successful copolymer formation. Each sample displayed a clear, unimodal shift toward lower retention times in GPC indicative of successful chain extension and gradient copolymer formation (Fig. 2a). Dynamic light scattering (DLS) was employed to determine the hydrodynamic diameter (D_h) of all TORC-NGs after CCL in both good and selective solvents (*i.e.*, chloroform and methanol, respectively; Fig. 2b and c) measured immediately following synthesis, prior to the dialysis procedures. The results revealed that the TORC-NGs remain intact in good solvents for both POEGMA and PGMA (chloroform) and have a larger hydrodynamic diameter than when dispersed in MeOH (selective solvent). This is hypothesized to

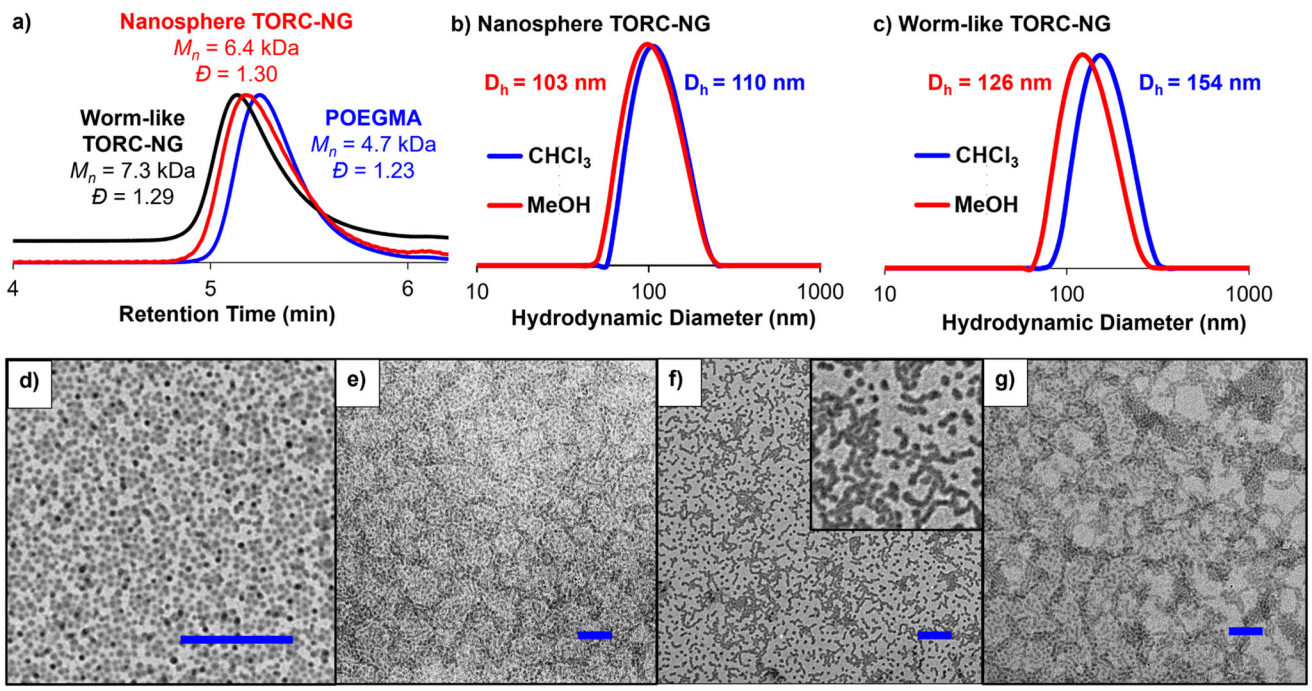

Fig. 2 PhotoATR-PISA fabrication of TORC-NGs with target DP(PGMA) = 86 for nanosphere and DP(PGMA) = 129 for worm-like showing clear shifts in the retention time *via* GPC (a). DLS of nanosphere (b) and worm-like (c) TORC-NGs provided evidence of TORC-CCL stabilization showing intact polymeric particles with larger hydrodynamic diameter when transferred to good solvent (*i.e.*, chloroform) and compared to selective solvent (*i.e.*, MeOH). This is confirmed *via* TEM of nanosphere (d, e) and worm-like (f, g) TORC-NGs cast onto grids from MeOH and $CHCl_3$, respectively (scale bars = 500 nm).

be due to unfolding/swelling of collapsed PGMA polymer chains within the aggregates as a result of favorable solvent–polymer interactions and is observed for both worm-like and nanosphere TORC-NGs. To confirm variations in TORC-NG morphology and stability, TEM was conducted for all PhotoATR-PISA reactions post TORC-CCL cast onto grids from MeOH and $CHCl_3$ (Fig. 2d–g) which further support enhanced stability of TORC-NGs.

To demonstrate UV-responsiveness, polymeric systems should be exposed to high energy UV-Light (λ_{max} = 254 nm), which may cause degradation in polymeric backbone. A series of polymers and copolymers were synthesized and exposed to 254 nm UV light to confirm photostability within the typical window of irradiation during release experiments (*ca.* 1 h). The ^{1}H NMR spectra and GPC chromatograms of all POGMA and PGMA homopolymers and copolymers demonstrated no significant main chain scission or degradation occurs upon irradiation (Fig. S10–15†). Furthermore, the photostability of Nile Red was studied under similar conditions revealing insignificant photobleaching after 1 h irradiation with 254 nm UV light (Fig. S16†).

Acid-induced solubility switching of PGMA cores

Upon ring opening of the epoxide PGMA pendant groups, the hydrophobic cores of TORC-NGs transform into hydrophilic poly(glycerol methacrylate) (PGlyMA), thus creating an imbalance in the hydrophilic/lipophilic ratio to cause disruption of the polymeric dispersion (*i.e.*, disassembly). Based on this hypothesis, with TORC-CCLs present, the ring-opening hydrolysis should cause the TORC-NGs to absorb more water and swell while remaining intact (Fig. 3a). Moreover, if no TORC-CCLs are present (*i.e.*, control non-CCL nanospheres in Fig. 3), the acid-catalyzed ring opening of epoxides should induce complete disassembly of nanoparticles generated *via* PhotoATR-PISA.

In order to confirm this hypothesis, the size and presence of nanoparticles was monitored by TEM and DLS (Fig. 3b and c, respectively). The nanoparticle (both TORC-NG and control non-CCL nanospheres) solutions were diluted (c = 0.2 mg mL^{-1}) with HCl/H_2O (adjusted to pH = 4.0) and the size of the micellar assemblies were measured after 24 h at room temperature. *Via* DLS, nanosphere TORC-NGs showed a distinct increase in diameter from D_h = 103 to 137 nm upon hydrolysis due to higher swelling ratio of the hydrophilic PGlyMA core (Fig. 3c). Similar swelling was observed *via* DLS analysis of worm-like TORC-NGs with increasing D_h = 126 to 141 nm upon acid-catalyzed PGMA hydrolysis.

The hydrolysis of the PGMA nanoparticle cores is further confirmed using a control, non-CCL nanosphere derivative also synthesized using one-pot PhotoATR-PISA. For this material, in the absence of TORC-CCL stabilization, the hydrolysis of PGMA to PGlyMA initiated a dramatic reduction in hydrodynamic diameter from D_h = 85.9 nm associated with the small nanosphere diameters in the assembly to D_h = 32.8 nm suggesting nearly complete disassembly of control nanoparticles. TEM also further supports the described hypothesis. TEM images of worm-like TORC-NGs cast from MeOH as-prepared and from HCl/H_2O display similar sizes and morphologies. However, after exposure to an acidic environment, control nanoparticles become particularly difficult to detect under an electronic microscope again suggesting disassembly. Finally, this hydrolysis was further confirmed using ^{1}H NMR showing corresponding chemical shifts associated with the formation of PGlyMA (Fig. S17†).

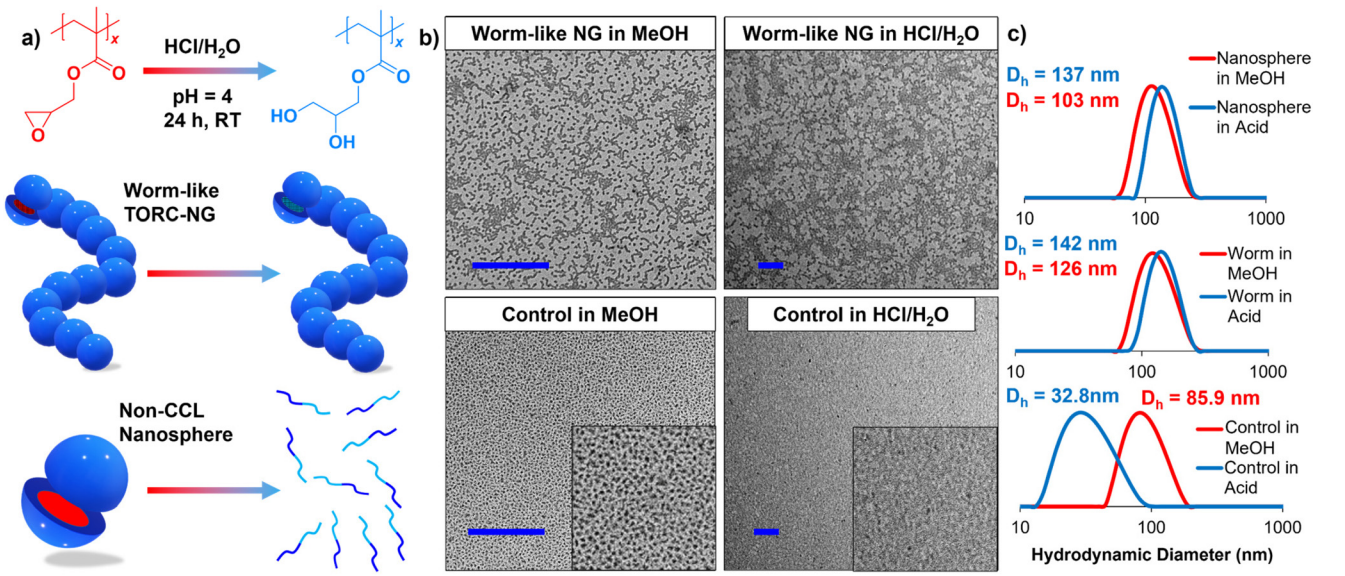

Fig. 3 Acid-catalysed hydrolysis of PGMA pendant epoxide rings in HCl/H_2O (pH = 4) which causes TORC-NGs to swell and non-CCL nanospheres to fully disassemble (a). This is confirmed *via* TEM of worm-like TORC-NGs and non-CCL nanosphere controls in MeOH and after reacting in HCl/H_2O for 24 h (b; scale bars = 500 nm; insets = 500 × 500 nm). This is confirmed *via* DLS through observed swelling of D_h after hydrolysis for TORC-NGs and decreases in D_h for non-CCL nanospheres due to disassembly (c).

Multi-stimuli responsive cargo release from Nile Red-loaded TORC-NGs

TORC-NG materials, after dialysis, were partitioned into various reactions to be exposed to combinations of acidic (*via* addition of HCl), reductive (*via* introducing DTT or GSH), and/or irradiative (*via* application of 254 nm UV light) environments and the release of Nile Red was monitored *via* fluorescence spectroscopy. Firstly, the release characteristics of TORC-NGs compared to non-CCL nanospheres were examined. TORC-NGs outperform control non-CCL nanospheres in terms of long-term integrity and slow release (Fig. 4). Encapsulated TORC-NGs (nanosphere and worm-like) exhibited a high level of stability (Fig. 4a and b) over the 72 h duration when no stimuli were applied with only ~5% release. In contrast, the non-CCL nanospheres demonstrated significant release even in neutral conditions (Fig. 4c) with nearly 55% release of Nile red in only 1 h.

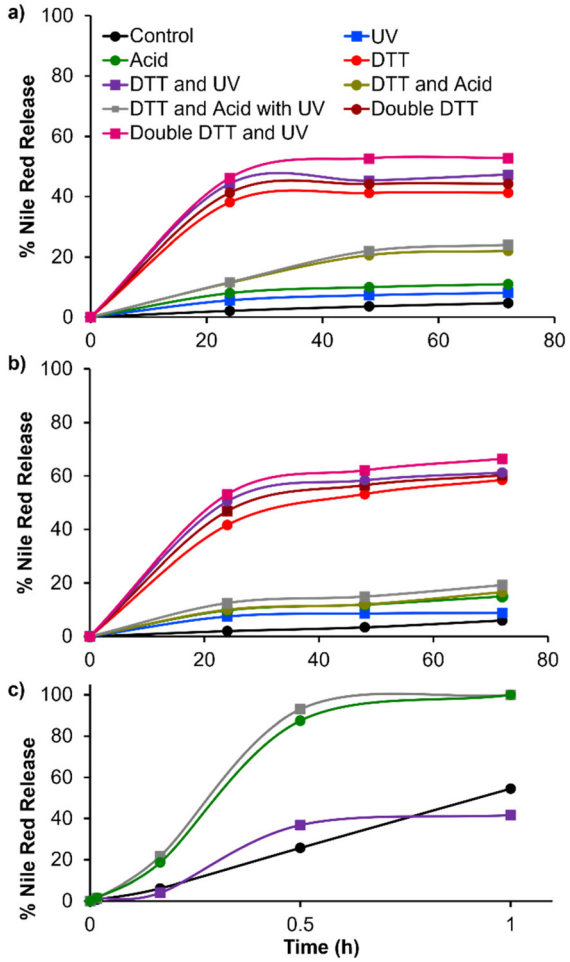

Fig. 4 Nile red release profiles for spherical TORC-NGs (a), worm-like TORC-NGs (b) and non-CCL nanosphere (c) upon application of various stimuli simultaneously (legend applies to all plots; control = no stimuli; acid = adjusted to pH 4 with HCl/H_2O; DTT = addition of 66.2 mM DTT for spherical TORC-NG and 51.1 mM DTT for worm-like TORC-NG; UV = 1 h irradiation with 254 nm UV light).

To further confirm the influence of PGMA hydrolysis and nanoparticle disassembly on release characteristics, TORC-NGs and non-CCL nanospheres were exposed to HCl/H_2O solutions adjusting solution pH = 4 and the Nile Red release was again monitored *via* fluorescence spectroscopy. Consistent with our previous results, acidic environments enabled rapid release of Nile Red (>99% after 1 h) from non-CCL nanospheres facilitated by the disassembly of the polymer nanoparticles upon hydrolysis. Furthermore, the release behavior for non-CCL nanospheres was monitored upon exposure to DTT and 254 nm UV light at pH = 7 showing similar profiles as controls (*i.e.*, no stimuli) with 41% release observed after 1 h. This value again increased greatly when solutions were adjusted pH = 4 with full release after 1 h demonstrating that pH is the only stimuli that influences release for non-CCL nanospheres.

The source of UV light for PhotoATR-PISA (λ = 365 nm) also facilitates CouMA dimerization for photo-responsive TORC-CCL incorporation (Scheme 1).[74,75] Photoinduced cleavage of the CouMA moieties is triggered upon UV-C (λ = 254 nm) irradiation as demonstrated by time-dependent UV-Vis spectra of as-prepared TORC-NGs upon UV irradiation (Fig. S18†). The increase of absorption peak at λ_{max} = 320 nm corresponds to photo-scission of coumarin methacrylate (*i.e.*, CCL reversal). Cleavage of the disulfide linkages was accomplished in the presence of DL-dithiothreitol (DTT) or glutathione (GSH) in aqueous solution. It should be noted that GSH is more hydrophilic than DTT and, as a result, diffusion of GSH into the hydrophobic core is hypothesized to be hampered (Fig. S19–24†). Because of this, TORC-NGs in the presence of GSH demonstrated significantly slower release (Fig. S21 and S24†). Each of these stimuli were investigated individually and collectively to determine their influence on Nile Red release characteristics.

For all applicable experiments, 254 nm UV light irradiation of TORC-NGs was conducted for only 1 h to prevent significant exposure of materials to the harsh UV conditions. This revealed only slight increases in release profile compared to controls without stimuli. After exposing nanosphere TORC-NGs to UV light, the release behavior was monitored over 72 h showing only 9.8% release with only the UV trigger (Fig. 4a). Worm-like TORC-NGs displayed very similar behaviors with only 9.0% Nile Red release after 72 h following irradiation for 1 h (Fig. 4b). The release profiles for both TORC-NG samples were also monitored in acidic environments (pH = 4) with no stimuli (green curves) showing only minimal increases in release with 11% and 15% release observed after 72 h incubation for nanosphere and worm-like TORC-NGs, respectively. This can be attributed to the fact that TORC-NGs only exhibit swelling behavior in acidic aqueous solutions or when triggered by UV light due to robust nature of their CCL structures without reversal of reductant-responsive CCLs.

Surprisingly, the release behavior of TORC-NGs triggered by disulfide reduction of CBMA CCLs in the presence of DTT alone (without UV), both at pH = 4 and 7, revealed relatively large release even without UV irradiation (yellow and red

curves, respectively). DTT was employed with a molar ratio of DTT : CBMA = 64 : 1. For both TORC-NGs, the majority of release observed occurred within the first 24 h after DTT exposure at pH = 7 (without UV irradiation) with nanosphere and worm-like materials exhibiting 38% and 42% Nile Red release, respectively. Surprisingly, disulfide reduction with DTT appeared hampered at pH = 4 leading to only 22% and 17% release after 72 h for nanosphere and worm-like TORC-NGs, respectively. Furthermore, the impact of DTT concentration on Nile red release was investigated. Increasing the molar ratio to twice the initial study at pH = 7 led to an enhanced release of 44% and 61% after 72 h for nanosphere and worm-like TORC-NGs, respectively.

These release characteristics were only slightly increased upon application of 1 h UV irradiation and DTT at pH = 7 leading to the 54% and 61% cargo release and pH = 4 leading to 24% and 19% release following 72 h incubation for nanosphere and worm-like TORC-NGs, respectively. The lower release in acidic environments is hypothesized to result from acid-catalyzed side reactions that occur between DTT and the PGMA cores. Under these conditions, where DTT and acid are introduced simultaneously, thiol-epoxide "click" reactions become favorable leading to rapid reaction of DTT with the PGMA cores leading to potentially irreversible CCLs to be installed. This is supported by ^{1}H NMR spectroscopy when reacting non-CCL nanospheres with DTT under similar aqueous conditions (Fig. S26 and 27†). Furthermore, disulfide exchange is well-known to be inhibited in acidic environments while facilitated in basic environments. For these reasons, the TORC-NGs are hypothesized to remain intact when all stimuli are applied together leading to only partial release of cargo. We postulated that application of stimuli in specific orders may result in quantitative release of cargo. Subsequent release experiments were conducted first exposing TORC-NGs to pH = 4 in HCl/H_2O solutions for set periods of time (*ca.* 72 h) followed by UV irradiation for 1 h and addition of DTT which demonstrated the expected AND-gate release behavior.

AND-gate controlled release *via* sequential addition of stimuli

To investigate the controlled AND-gate release behavior of TORC-NGs, specific experimental procedures were devised. In order to examine the sequential addition of stimuli starting first with acidification, a representative worm-like TORC-NG was selected (Fig. 5). For this, the TORC-NG was incubated in HCl/H_2O solutions at pH = 4 for 72 h to fully hydrolyze the PGMA cores to PGlyMA prior to application of UV light and/or DTT. Comparative analysis after acidification with the original sample revealed an 18% release, with the majority of the release occurring within 2 days (Fig. 5a and b).

Upon reaching the maximum release in the acidic environment after 72 h, the sample was divided into two separate vials. One was utilized to examine the redox responsiveness in the presence of DTT (c = 51.1 mM), while the other vial was subjected to 254 nm UV light exposure for 1 h. All samples were continuously monitored for a period of 3 days after stimuli *via* fluorescence spectroscopy. Upon addition of DTT following hydrolysis, significant Nile Red release (*ca.* 51%) was observed immediately after addition but this release quickly attenuated leading to minimal additional release over the subsequent 72 h (*ca.* ~4%) (Fig. 5a and d). In response to UV irradiation alone, similar behavior was noted with a sudden burst release during irradiation (*ca.* 55%) followed by complete stabilization and no subsequent release observed over the next 72 h (Fig. 5b and e).

In order to achieve enhanced AND-Gate release, the presence of all stimuli is imperative. Firstly, like before, the worm-like TORC-NG sample was subjected to acidic environment at pH = 4 upon addition of HCl leading to 17% release after incubating for 3 days, consistent with previous experiments (Fig. 5c and f). Subsequently, the sample was exposed to 254 nm UV light for 1 h, providing burst release of 58% of cargo, followed by addition of DTT leading to sustained release over the next 5 days with 83% total cargo release. The following days led to unexpected morphological transitions for worm-like TORC-NG samples (*vide infra*). Furthermore, alternative sequences of stimuli application were investigated, wherein the UV exposure preceded the acidic incubation, followed by the application of DTT at different pH. This alternative sequence also exhibited a substantial release of the target compound (81% over a period of 3 days; Fig. S28†). These results provide clear evidence that application of stimuli in specific orders, most notably acidification first, is required to access AND-gate release. Further, to achieve full release of cargo, the application of all stimuli is crucial.

Analogously, nanosphere TORC-NGs demonstrated a release efficiency = 93% under the same sequence of stimuli after incubation with DTT for 7 days (Fig. 6a and b). The release process was corroborated by both TEM and DLS analyses, which provided evidence of swelling, de-crosslinking, and disassembly. After purification *via* dialysis against water, the hydrodynamic diameter of the particles was measured and found to be smaller compared to methanol (D_h = 68.6 nm). Upon addition of HCl, the ring opening of PGMA pendant epoxide groups led to modest swelling effect as evidenced by DLS with slight increases in the D_h from 68.6 nm to 72.9 nm in water (Fig. 6c). Similarly, in THF, a good solvent for all polymer blocks, the D_h increased from the initial size of 134 nm to 218 nm upon exposure to HCl providing strong evidence that the TORC-NGs remained intact in the presence of the good solvent (Fig. 6d). Subsequent exposure to 254 nm UV light led to the de-crosslinking of the PCouMA CCLs resulting in a reduction of D_h = 64.5 nm in water and 106 nm in THF possibly due to the initial burst release of cargo. Further manipulation of the system involved the addition of DTT and subsequent incubation for 7 days. This led to a significant decrease in the nanoparticle size, with DLS measurements of D_h = 25.8 and 10 nm in water and THF, respectively, indicative of near complete disassembly of the spherical TORC-NG structures. TEM analysis was performed following disassembly confirming the absence of particles on the grid (Fig. S29†).

Worm-like TORC-NG demonstrated an 83% release during the first 5 days incubating with DTT, as discussed previously.

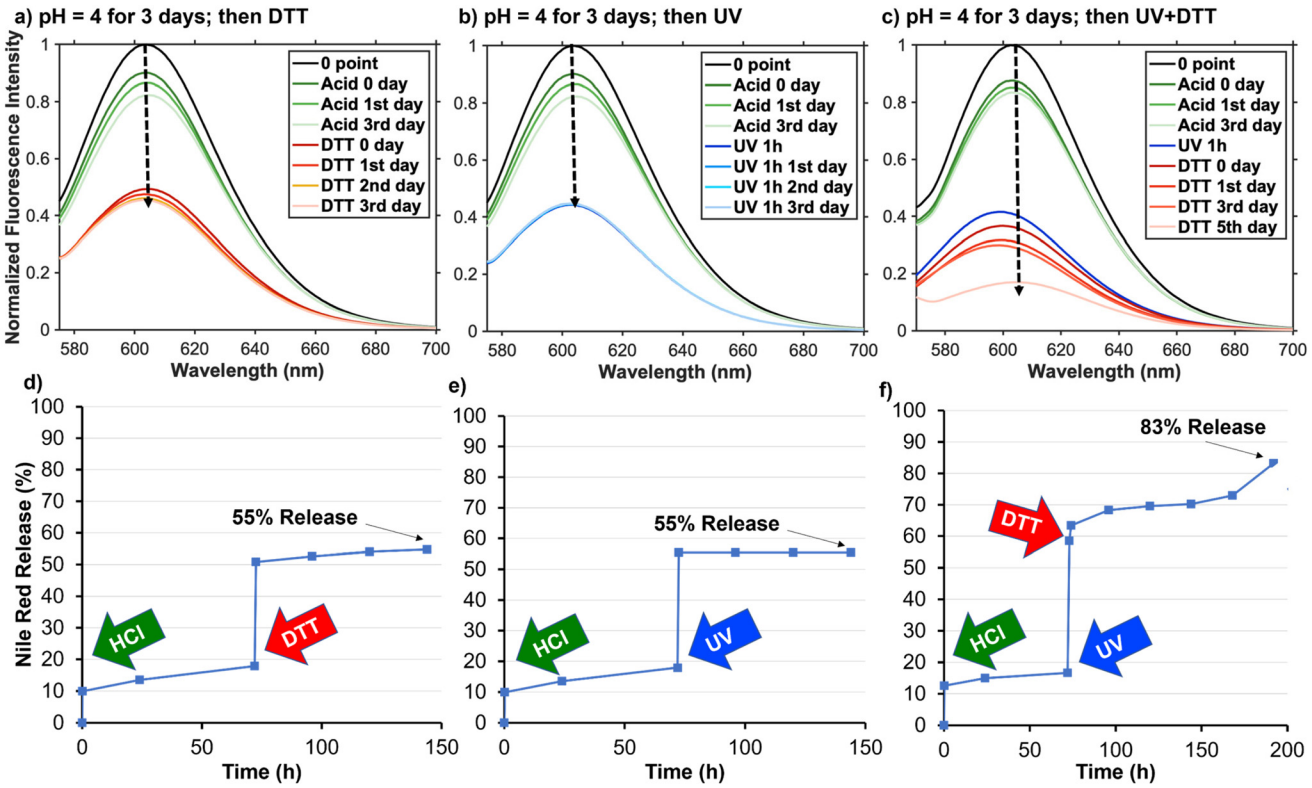

Fig. 5 Fluorescence spectra of Nile Red loaded, worm-like TORC-NGs after acidification to pH = 4 with HCl and incubating for 3 days followed by addition of DTT alone (c = 51.1 M; a, d), irradiation with 254 nm UV light for 1 h alone (b, e), or introduction of UV light and DTT sequentially (c, f) leading to AND-gate cargo release only when both stimuli were applied.

Notably, these materials displayed intriguing phenomena whereby an increase in fluorescent intensity was observed suddenly after 5 days (*i.e.*, re-encapsulation), followed by continued release over the course of 20 days (Fig. 7a and b). Utilizing TEM and DLS, it was revealed that the particles underwent similar swelling as with nanosphere TORC-NGs but no complete disassembly was observed. DLS analysis demonstrated a notable increase in size, indicating significant swelling of the nanoparticles upon acidification for 3 days. Specifically, the D_h of the sample in H_2O exhibited an increase from 105 nm to 121 nm, while the sample in THF showed an increase from D_h = 164 nm to 188 nm (Fig. 7f and g, respectively). Importantly, despite this swelling phenomenon, the nanoparticles remained structurally intact.

Subsequently, after 5 days incubation with DTT, reformation of longer worm-like micelle aggregates occurred, as evidenced by TEM and DLS analyses. *Via* DLS, we observed increases in D_h = 139 and 412 nm in H_2O and THF, respectively. Upon aggregation, these structures were found to re-encapsulate released Nile Red to some extent as evidenced by the increase in fluorescence emission intensity revealing a decrease in total dispersed Nile Red from 83% to 60%. The release study was extended to 15 additional days revealing slow, sustained release throughout this timeframe reaching 80% after 20 total days incubating with DTT. Unlike with nanosphere TORC-NGs, complete disassembly was not observed *via* DLS or TEM, revealing similarly sized nanoparticles to the initial and significant disaggregation of the long worm-like micelle nanostructures (Fig. 7c–e). DLS analysis revealed a reduction in nanoparticle size in both solvents, D_h measurements showed a decrease to 127 nm in H_2O and 198 nm in THF (Fig. 7f and g) after 20 days incubation.

The release characteristics for TORC-NGs were also monitored at various pH levels readjusting pH = 7 and 9 with NaOH during DTT additions to observe how this affects final release kinetics (Fig. S30 and S31†). The findings indicated that acidic environment at pH = 4 exhibited greater release effectiveness for both morphologies but with very similar trends. Notably, the worm-like TORCNG demonstrated consistent behavior of re-encapsulation across all tested environments.

Formation of TORC-NG tubesomes and Nile Red release

Polymeric vesicles (also known as polymersomes) stand out among nanostructures due to their distinct structures and potential applications in controlled release, drug delivery, and bio-related materials. The ability of amphiphilic copolymer polymersomes to encapsulate both hydrophilic agents in the aqueous core and hydrophobic compounds within the membrane is unique. In this work, we applied our described strategies for the synthesis of TORC-NG polymersomes. Because CBMA has a lower reactivity than methacrylate monomer, the cross-linking process of CBMA was delayed to the late stage of

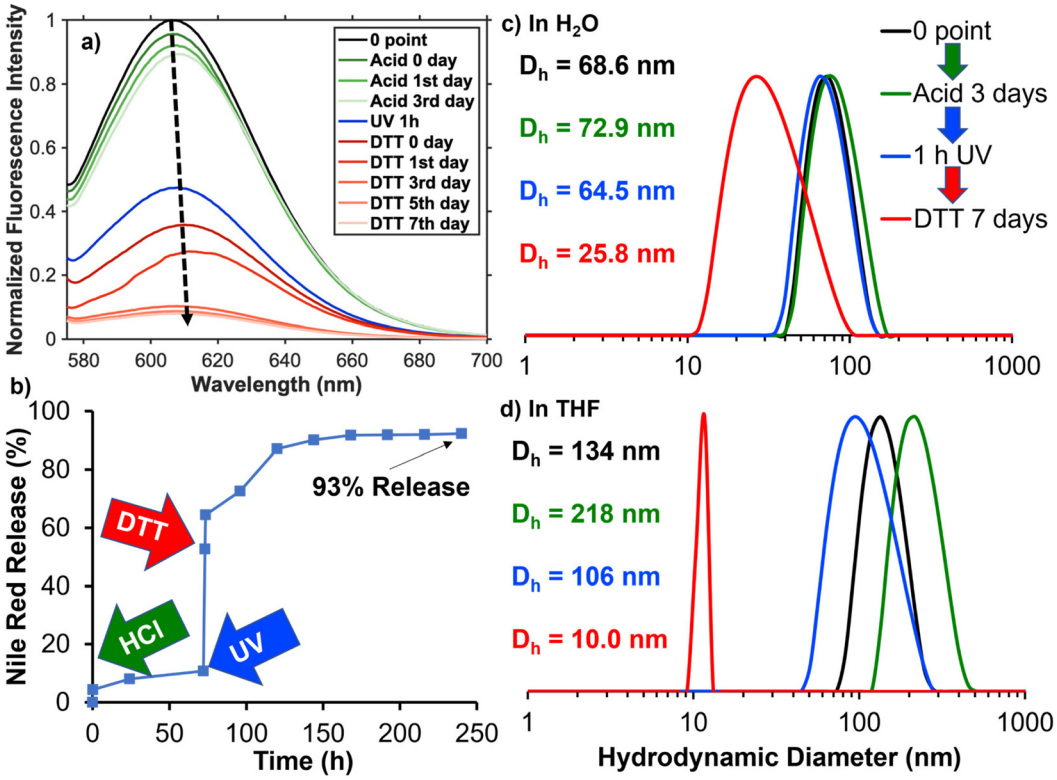

Fig. 6 Stimuli-triggered Nile Red release from nanosphere TORC-NGs upon sequential addition of HCl (acidification to pH = 4 for 3 days) followed by 1 h irradiation with 254 nm UV light, subsequent addition of 66.2 mM DTT and incubation for 7 days as monitored by fluorescence spectroscopy (a, b). DLS was also conducted to track the sizes of nanosphere TORC-NGs after adding different stimuli in H_2O (c) and THF (d).

polymerization after the formation of polymersomes allowing for sufficient morphological transitions to take place prior to fixing the nanogel morphology *via* CCL.

To access these morphologies, we altered the core-forming segments from PGMA to PBMA due to our previous difficulties in forming higher-order morphologies using PGMA alone (Scheme S1†).[70] Furthermore, we performed PhotoATR-PISA in two pots, starting with macroinitiator synthesis and purification prior to PISA to allow for more precise control to hydrophililc/lipophilic ratios. The morphology evolved slowly due to the presence of CBMA at the start of the PhotoATR-PISA reaction and the gradual polymerization of this crosslinker. At ~50% BMA conversion, the second CouMA crosslinker was added to the system, and the reaction proceeded for an additional 7 days until full BMA, CBMA and CouMA conversion. Interestingly, the TORC-NG that resulted proceeded through more typical spherical polymersome structures at early stages of CBMA crosslinking (*ca.* 69% conversion at 40 h reaction; Fig. S32;† Fig. 8a) and transitioned to multi-micron long tubesome nanostructures after full CBMA conversion in 7 days (Fig. 8b). As depicted, these anisotropic TORC-NGs exhibit a wide range of lengths and widths with averages for each = 1.13 and 4.22 μm. Again, solvent switches to good solvents for both blocks were performed to examine the stability of tubesome TORC-NGs to environmental perturbations. Analysis of these materials cast from $CHCl_3$, even in early stages of CBMA conversion, revealed intact tubesome nanostructures, as evidenced by TEM (Fig. 8c and d). This was also confirmed *via* DLS which showed an increase in D_h = 205 nm to 480 nm upon solvent switch from methanol to $CHCl_3$ despite the block copolymer solubility in chloroform (Fig. S34†). The longer tubesome structures were also confirmed when cast from $CHCl_3$ after full conversion (7 days).

Again, we studied the release characteristics of Nile Red loaded tubesome TORC-NGs using fluorescence spectroscopy. The release profile of this system (Fig. S35†) was far slower and incomplete when compared to nanosphere and worm-like morphologies due to lack of solubility switchable groups in the cores of TORC-NGs. As expected, when both redox (DTT) and UV stimuli were applied together, maximum release was recorded, providing additional evidence of AND-gate release albeit to a far less extent than the other analogues. When all three stimuli were incorporated (redox, UV, and acid), the release profile accelerated slower than at neutral pH but reaches a similar maximum release in 72 h (*ca.* 27% release efficiency). The most significant difference between PBMA-based tubesome TORC-NGs and PGMA-based TORC-NGs is the effect of acidic environments. The absence of reactive epoxides in the core provides no solubility switchable handle induced by decreases in pH. This method, however, provides a unique route to large tubesome structures, a morphology rare to PISA methodologies, with orthogonal, dynamic CCLs. This develop-

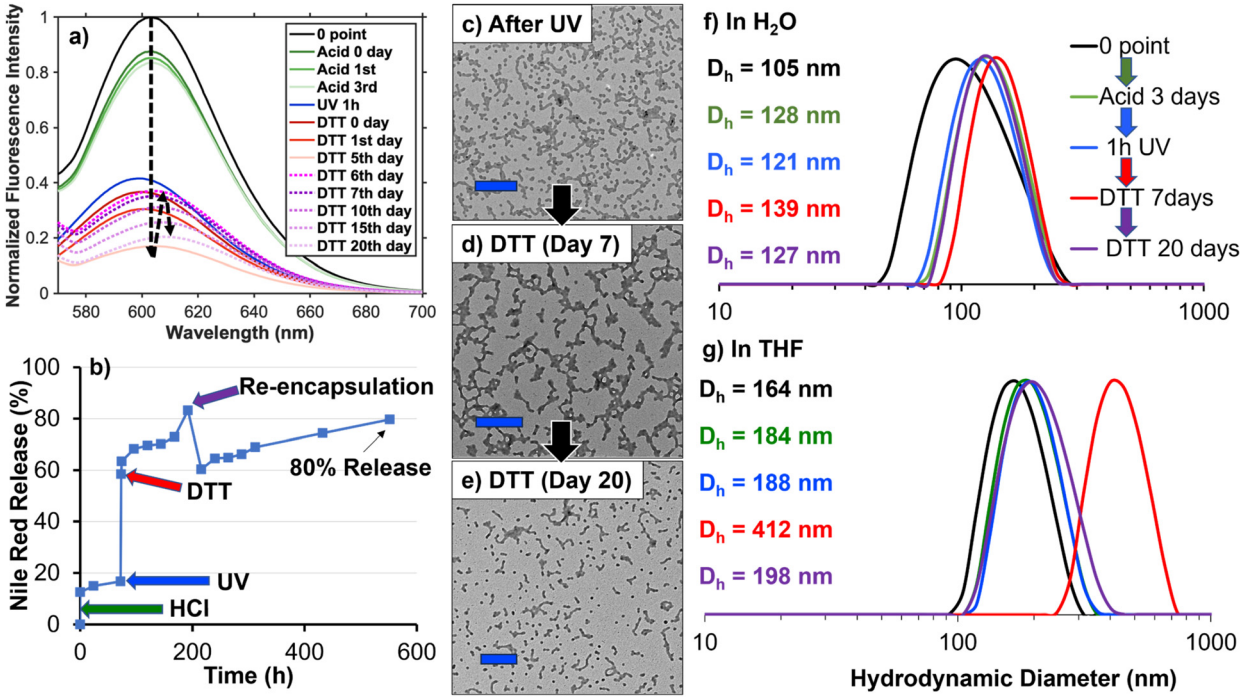

Fig. 7 Stimuli-triggered Nile Red release from worm-like TORC-NGs upon sequential addition of HCl (acidification to pH = 4 for 3 days) followed by 1 h irradiation with 254 nm UV light, addition of 51.1 mM DTT and incubation for 20 days as monitored by fluorescence spectroscopy (a, b). This revealed, at day 5+, sudden re-encapsulation of Nile Red induced by morphological transitions from short to long worm-like nanostructures followed by the slower breakdown of long worms to short worms over the next 15 days as evidenced by TEM (c–e; scale bars = 500 nm). DLS was also conducted to track the sizes of worm-like TORC-NGs after adding different stimuli in H_2O (f) and THF (g).

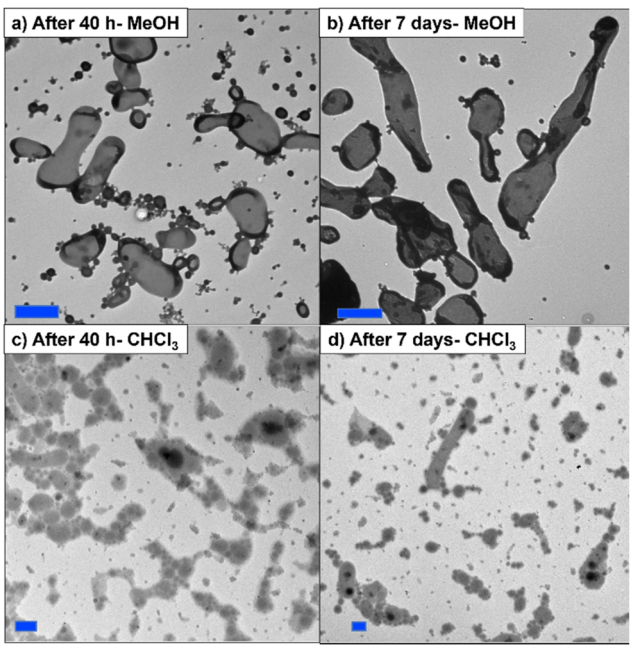

Fig. 8 TEM images of PBMA-*b*-POEGMA vesicle TORC-NGs as conversion of CBMA increases showing large, elliptical polymersomes at low conversions (a) that transition to large, multi-micron long tubesome structures at full CBMA conversion (b). The stability of these materials at both stages is confirmed upon solvent switch to $CHCl_3$ and imaging using TEM (c, d; all scale bars = 2.0 μm).

ment expands the toolbox of bottom-up nanogel fabrication and provides a facile route to various CCL nanomaterials for a variety of applications. Furthermore, the installed responsiveness of TORC-CCLs is expected to hold applicability for cancer treatment due to the acidic and reductive environments of most tumor providing necessary conditions for reducing disulfides and hydrolyzing PGMA cores. The final application of UV-light can be accomplished using NIR laser irradiation coupled with upconversion within nanocomposites and will be accomplished in future work.

Conclusions

In this study, the incorporation of TORC-CCLs into the cores polymeric nanogels provided streamlined routes to multi-stimuli responsive polymeric nanomaterials with high stabilities and encapsulation efficiencies. Upon addition of specific stimuli (*i.e.*, acid, redox, UV) in specific orders, high release efficiencies are possible through acid-catalyzed hydrolytic ring-opening reactions in PGMA cores and TORC-CCL bond reversal in response to DTT and 254 nm UV light. Implementation of CouMA allowed for the installation of photo-responsive TORC-CCLs *via* [2 + 2] cycloaddition reactions between coumarin pendants induced by 365 nm UV light used in PhotoATR-PISA. The slow incorporation of CBMA allows for late-stage crosslinking providing sufficient opportunities for

morphology evolution. These TORC-NG materials were synthesized with nanosphere, worm-like and tubesome morphologies and displayed morphology-tunable release behaviors. Moreover, when first exposed to acidic environments at pH = 4 to hydrolyze cores of PGMA-based TORC-NGs, the release behavior can be tuned allowing for partial burst release of cargo when exposed to a single stimuli (*i.e.*, UV or DTT) and more extensive, sustained, AND-gate release when exposed to both stimuli. These materials and methods provide simple, one-pot routes to TORC-NG materials with multi-responsivity and offer room for improvement *via* introduction of additional TORC-CCLs increasing complexity, a topic currently under investigation.

Conflicts of interest

There are no conflicts to declare.

Acknowledgements

This material is based upon work supported by the National Science Foundation under Grant 2125727, and any opinions, findings, and conclusions, or recommendations expressed in this material are those of the author(s) and do not necessarily reflect the views of the National Science Foundation.

References

1 X. Fu, L. Hosta-Rigau, R. Chandrawati and J. Cui, *Chem*, 2018, **4**, 2084–2107.
2 D. Astruc and F. Chardac, *Chem. Rev.*, 2001, **101**, 2991–3024.
3 J.-L. Li, R. Bai and B.-H. Chen, *Langmuir*, 2004, **20**, 6068–6070.
4 Q. Zhang, Y. Zhang, Y. Wan, W. Carvalho, L. Hu and M. J. Serpe, *Prog. Polym. Sci.*, 2021, **116**, 101386.
5 L. Hu, Q. Zhang, X. Li and M. J. Serpe, *Mater. Horiz.*, 2019, **6**, 1774–1793.
6 J. Tang, P. J. Quinlan and K. C. Tam, *Soft Matter*, 2015, **11**, 3512–3529.
7 A. Klaikherd, C. Nagamani and S. Thayumanavan, *J. Am. Chem. Soc.*, 2009, **131**, 4830–4838.
8 M. A. C. Stuart, W. T. Huck, J. Genzer, M. Müller, C. Ober, M. Stamm, G. B. Sukhorukov, I. Szleifer, V. V. Tsukruk and M. Urban, *Nat. Mater.*, 2010, **9**, 101–113.
9 P. Theato, B. S. Sumerlin, R. K. O'Reilly and T. H. Epps III, *Chem. Soc. Rev.*, 2013, **42**, 7055–7056.
10 H. M. Seifert, K. Ramirez Trejo and E. V. Anslyn, *J. Am. Chem. Soc.*, 2016, **138**, 10916–10924.
11 J. F. Reuther, S. D. Dahlhauser and E. V. Anslyn, *Angew. Chem., Int. Ed.*, 2019, **58**, 74–85.
12 Y. Hai, H. Zou, H. Ye and L. You, *J. Org. Chem.*, 2018, **83**, 9858–9869.
13 H. Yang, S. Ghiassinejad, E. Van Ruymbeke and C.-A. Fustin, *Macromolecules*, 2020, **53**, 6956–6967.
14 I. W. Moran, M. M. Sprachman, J. L. Bachman, S. D. Dahlhauser, E. V. Anslyn and D. J. Carter, *Bioconjugate Chem.*, 2020, **31**, 2191–2200.
15 J. Mao, Y. Hai, H. Ye and L. You, *J. Org. Chem.*, 2020, **85**, 5351–5361.
16 M. R. Arkenberg, H. D. Nguyen and C.-C. Lin, *J. Mater. Chem. B*, 2020, **8**, 7835–7855.
17 H. Zou, Y. Hai, H. Ye and L. You, *J. Am. Chem. Soc.*, 2019, **141**, 16344–16353.
18 A. Wilson, G. Gasparini and S. Matile, *Chem. Soc. Rev.*, 2014, **43**, 1948–1962.
19 A. Abdollahi, H. Roghani-Mamaqani, B. Razavi and M. Salami-Kalajahi, *Polym. Chem.*, 2019, **10**, 5686–5720.
20 J. M. Schumers, C. A. Fustin and J. F. Gohy, *Macromol. Rapid Commun.*, 2010, **31**, 1588–1607.
21 C. De las Heras Alarcón, S. Pennadam and C. Alexander, *Chem. Soc. Rev.*, 2005, **34**, 276–285.
22 O. Bertrand and J.-F. Gohy, *Polym. Chem.*, 2017, **8**, 52–73.
23 A. Abdollahi, A. R. Mahdavian and H. Salehi-Mobarakeh, *Langmuir*, 2015, **31**, 10672–10682.
24 J. Lee, M. V. Maddipatla, A. Joy and B. D. Vogt, *Macromolecules*, 2014, **47**, 2891–2898.
25 M. V. Maddipatla, D. Wehrung, C. Tang, W. Fan, M. O. Oyewumi, T. Miyoshi and A. Joy, *Macromolecules*, 2013, **46**, 5133–5140.
26 Y. Huang, R. Dong, X. Zhu and D. Yan, *Soft Matter*, 2014, **10**, 6121–6138.
27 M. Talelli, M. Barz, C. J. Rijcken, F. Kiessling, W. E. Hennink and T. Lammers, *Nano Today*, 2015, **10**, 93–117.
28 Z. Abousalman-Rezvani, P. Eskandari, H. Roghani-Mamaqani and M. Salami-Kalajahi, *Carbohydr. Polym.*, 2019, **225**, 115247.
29 Z. Abousalman-Rezvani, P. Eskandari, H. Roghani-Mamaqani, H. Mardani and M. Salami-Kalajahi, *Polymer*, 2019, **182**, 121830.
30 Z. Du, X. Yan, R. Dong, K. Ke, B. Ren and Z. Tong, *Macromolecules*, 2018, **51**, 1518–1528.
31 J. Ling, M. Z. Rong and M. Q. Zhang, *Polymer*, 2012, **53**, 2691–2698.
32 S. Banerjee, R. Tripathy, D. Cozzens, T. Nagy, S. Keki, M. Zsuga and R. Faust, *ACS Appl. Mater. Interfaces*, 2015, **7**, 2064–2072.
33 M. A. Azagarsamy, D. D. McKinnon, D. L. Alge and K. S. Anseth, *ACS Macro Lett.*, 2014, **3**, 515–519.
34 D. S. Shin, J. You, A. Rahimian, T. Vu, C. Siltanen, A. Ehsanipour, G. Stybayeva, J. Sutcliffe and A. Revzin, *Angew. Chem.*, 2014, **126**, 8360–8363.
35 M. H. Lee, Z. Yang, C. W. Lim, Y. H. Lee, S. Dongbang, C. Kang and J. S. Kim, *Chem. Rev.*, 2013, **113**, 5071–5109.
36 C.-K. Chen and S.-C. Huang, *Mol. Pharm.*, 2016, **13**, 4152–4167.
37 P. Zhang, J. Wu, F. Xiao, D. Zhao and Y. Luan, *Med. Res. Rev.*, 2018, **38**, 1485–1510.

38 S. A. Elkassih, P. Kos, H. Xiong and D. J. Siegwart, *Biomater. Sci.*, 2019, **7**, 607–617.
39 T. Fuoco, D. Pappalardo and A. Finne-Wistrand, *Macromolecules*, 2017, **50**, 7052–7061.
40 C.-K. Chen, M.-G. Liao, Y.-L. Wu, Z.-Y. Fang and J.-A. Chen, *Mol. Pharm.*, 2020, **17**, 3461–3476.
41 D. Yang and R. H. Pelton, *ACS Sustainable Chem. Eng.*, 2017, **5**, 10544–10550.
42 G. L. Grocke, H. Zhang, S. S. Kopfinger, S. N. Patel and S. J. Rowan, *ACS Macro Lett.*, 2021, **10**, 1637–1642.
43 H. Sun, F. Meng, R. Cheng, C. Deng and Z. Zhong, *Acta Biomater.*, 2014, **10**, 2159–2168.
44 Y. Fang, W. Yang, L. Cheng, F. Meng, J. Zhang and Z. Zhong, *Acta Biomater.*, 2017, **64**, 323–333.
45 J. Michalska-Walkowiak, B. Förster, S. Hauschild and S. Förster, *Adv. Mater.*, 2022, **34**, 2108833.
46 S. Uchiyama, N. Kawai, A. P. de Silva and K. Iwai, *J. Am. Chem. Soc.*, 2004, **126**, 3032–3033.
47 C. Rullyani, M. Singh, S.-H. Li, C.-F. Sung, H.-C. Lin and C.-W. Chu, *Org. Electron.*, 2020, **85**, 105818.
48 I. Piergentili, P. R. Bouwmans, L. Reinalda, R. W. Lewis, B. Klemm, H. Liu, R. M. de Kruijff, A. G. Denkova and R. Eelkema, *Polym. Chem.*, 2022, **13**, 2383–2390.
49 Y. Dong, X. Ma, H. Huo, Q. Zhang, F. Qu and F. Chen, *J. Appl. Polym. Sci.*, 2018, **135**, 46675.
50 C. Wei, J. Guo and C. Wang, *Macromol. Rapid Commun.*, 2011, **32**, 451–455.
51 X. Chen, A. H. Soeriyadi, X. Lu, S. M. Sagnella, M. Kavallaris and J. J. Gooding, *Adv. Funct. Mater.*, 2014, **24**, 6999–7006.
52 R. Cheng, F. Meng, C. Deng, H.-A. Klok and Z. Zhong, *Biomaterials*, 2013, **34**, 3647–3657.
53 B. A. Badeau, M. P. Comerford, C. K. Arakawa, J. A. Shadish and C. A. DeForest, *Nat. Chem.*, 2018, **10**, 251–258.
54 E. A. Mahmoud, J. Sankaranarayanan, J. M. Morachis, G. Kim and A. Almutairi, *Bioconjugate Chem.*, 2011, **22**, 1416–1421.
55 M. Cai, Y. Ding, L. Wang, L. Huang, X. Lu and Y. Cai, *ACS Macro Lett.*, 2018, **7**, 208–212.
56 A. Shahrokhinia, R. A. Scanga, P. Biswas and J. F. Reuther, *Macromolecules*, 2021, **54**, 1441–1451.
57 F. L. Hatton, J. R. Lovett and S. P. Armes, *Polym. Chem.*, 2017, **8**, 4856–4868.
58 S. J. Byard, M. Williams, B. E. McKenzie, A. Blanazs and S. P. Armes, *Macromolecules*, 2017, **50**, 1482–1493.
59 L. Qiu, C. R. Xu, F. Zhong, C. Y. Hong and C. Y. Pan, *Macromol. Chem. Phys.*, 2016, **217**, 1047–1056.
60 M. Chen, J.-W. Li, W.-J. Zhang, C.-Y. Hong and C.-Y. Pan, *Macromolecules*, 2019, **52**, 1140–1149.
61 A. Anastasaki, B. Oschmann, J. Willenbacher, A. Melker, M. H. Van Son, N. P. Truong, M. W. Schulze, E. H. Discekici, A. J. McGrath and T. P. Davis, *Angew. Chem., Int. Ed.*, 2017, **56**, 14483–14487.
62 A. Anastasaki, V. Nikolaou, N. W. McCaul, A. Simula, J. Godfrey, C. Waldron, P. Wilson, K. Kempe and D. M. Haddleton, *Macromolecules*, 2015, **48**, 1404–1411.
63 X. Pan, N. Malhotra, A. Simakova, Z. Wang, D. Konkolewicz and K. Matyjaszewski, *J. Am. Chem. Soc.*, 2015, **137**, 15430–15433.
64 Z. Wang, X. Pan, J. Yan, S. Dadashi-Silab, G. Xie, J. Zhang, Z. Wang, H. Xia and K. Matyjaszewski, *ACS Macro Lett.*, 2017, **6**, 546–549.
65 S. Chantasirichot, Y. Inoue and K. Ishihara, *Polymer*, 2015, **61**, 55–60.
66 J. F. Lutz, *J. Polym. Sci., Part A: Polym. Chem.*, 2008, **46**, 3459–3470.
67 L.-Y. Qi, Y. Wang, L.-F. Hu, P.-S. Zhao, H.-Y. Yu, L. Xing, X.-D. Gao, Q.-R. Cao and H.-L. Jiang, *J. Controlled Release*, 2022, **341**, 511–523.
68 Q. Jin, F. Mitschang and S. Agarwal, *Biomacromolecules*, 2011, **12**, 3684–3691.
69 J. Dou, R. Yang, K. Du, L. Jiang, X. Huang and D. Chen, *Polym. Chem.*, 2020, **11**, 3296–3304.
70 A. Shahrokhinia, S. Rijal, B. Sonmez Baghirzade, R. A. Scanga, P. Biswas, S. Tafazoli, O. G. Apul and J. F. Reuther, *Macromolecules*, 2022, **55**, 3699–3710.
71 A. F. Cardozo, C. Julcour, L. Barthe, J.-F. Blanco, S. Chen, F. Gayet, E. Manoury, X. Zhang, M. Lansalot and B. Charleux, *J. Catal.*, 2015, **324**, 1–8.
72 W.-J. Zhang, C.-Y. Hong and C.-Y. Pan, *Biomacromolecules*, 2016, **17**, 2992–2999.
73 S. Sugihara, S. P. Armes, A. Blanazs and A. L. Lewis, *Soft Matter*, 2011, **7**, 10787–10793.
74 T. Wolff and H. Görner, *Phys. Chem. Chem. Phys.*, 2004, **6**, 368–376.
75 N. K. Mal, M. Fujiwara and Y. Tanaka, *Nature*, 2003, **421**, 350–353.